Setting Systematic Error Requirements on the CGEM Telescope Using B Mode Contamination Criteria

by

Artem Davydov

A THESIS SUBMITTED IN PARTIAL FULFILLMENT OF
THE REQUIREMENTS FOR THE DEGREE OF

BACHELOR OF SCIENCE

in

The Faculty of Science

(Physics and Astronomy)

THE UNIVERSITY OF BRITISH COLUMBIA

(Vancouver)

April 2021

Abstract

The Canadian Galactic Emission Mapper (CGEM) is a planned radio telescope that will map the polarized 10GHz northern hemisphere sky. One of the main science goals of the experiment to improve our foreground modeling capabilities in support of the search for the B mode. I created a Python simulator that produces data streams given a scan strategy and incorporates a realistic hat-feed antenna beam response. The data streams are then fed to a map maker that successfully reconstructed the Stokes T, Q, and U as seen by CGEM. We computed the BB power spectra of the recovered sky maps extrapolated to the CMB observation window (150GHz) with: the full co pol and cross pol patterns, and only the co pol beam pattern incorporated into the simulation. We also produced BB power spectra for the input maps convolved to 1° resolution corresponding to the main lobe of the cross pol. We found that the overall effect of the full co and cross pol beam pattern is a BB power reduction on order of $10^{-4}\mu K^2$ for $\ell < 10$ and decreases with higher ℓ. The contamination due to the beam response is lower than the CMB B mode power for r = 0.1. This result may imply that the overall contribution of the beam pattern to BB confusion is low, strengthening the hat-feed as the lead candidate for the antenna design. There is an important caveat in the power spectrum analysis procedure. The cross pol beam pattern was implemented as if it was circularly symmetric. However we know that the phase of the potential hat feed cross pol depends on the ϕ cut of the beam pattern. The implementation of a ϕ dependent cross pol response is a topic of active discussion in the CGEM group. Future iterations of the pipeline will include electronic systematic effects such as phase and gain errors and a properly incorporated cross pol effect.

Table of Contents

List of Figures

Acknowledgements

I would like to thank my supervisor Dr. Gary Hinshaw. I am grateful for the opportunity to work with the CGEM group. I would also like to thank my second reader Dr. Mark Halpern for his valuable feedback. I want to thank Dr. Rob Kiefl for his guidance and support throughout PHYS349. Finally, I want to thank Josh MacEachern for his mentorship throughout my summer research and directed research course.

Chapter 1

Introduction

1.1 Motivation

The Cosmic Microwave Background (CMB) propagates to us from all directions and carries information about the primordial universe. The CMB polarization field can be decomposed into a curl-like field, the B-mode, and the gradient-like field, the E-mode. The B-mode imprinted on the CMB could only be sourced by gravitational waves present in the universe after decoupling. These gravitational waves are theorized to have been sourced by a rapid period of expansion called inflation. The inflationary theory of the universe solves important problems in cosmology however it was never observed directly. Detection of the B-mode will provide supporting "smoking gun" evidence for the theory of inflation.

Polarized emission from our Galaxy swamps the signal and makes direct detection of the B-mode extremely difficult. The removal of the foreground from CMB surveys requires an understanding of the spatial and spectral variation of different foreground emission components across a wide frequency band. The Canadian Galactic Emission Mapper is a planned radio telescope that will map the intensity and polarization of the Northern Hemisphere sky at 10GHz, where emission is dominated by Synchrotron radiation. CGEM data will provide additional information about the polarized Galactic Synchrotron emission which will help us better model the individual components of the polarized foreground.

The Astro2020 APC white paper addresses the current limitations of CMB experiments and outlines a guiding philosophy for upcoming instruments. The expected level of CMB B mode rms temperature brightness fluctuations given r 10^{-4} are in the nK regime[15]. In order for the CGEM polarization maps to be useful to foreground cleaning we have to target a nK level sensitivity in the CMB observation window frequency (100-150GHz). My project will support CGEM design decisions and will set instrument specifications using simulations and data analysis. I will explore the effects of systematic errors on the extrapolated power spectrum of mock CGEM observations to assess their possible impact on CMB B mode detection.

Chapter 2

Theory

2.1 ΛCDM: The Cold Dark Matter Model

One of the leading models of cosmology is The Cold Dark Matter (ΛCDM) model. ΛCDM incorporates the big bang as the initial event which followed by a rapid period of expansion known as inflation. The model explains how inflation transforms quantum fluctuations in the universe into macro structures in our observable universe and how inflation gives rise to the Cosmic Microwave Background and its anisotropy[5].

2.2 The Cosmic Microwave Background (CMB)

The CMB was first discovered by Arno Penzias and Robert Wilson of Bell labs in 1965. They used a 20-foot horn reflector in Holmdel, New Jersey. They noticed an excess antenna temperature that is unaccounted for by systematic of seasonal effects[13]. The cosmic microwave background is relic radiation propagating to us from all directions from the surface of last scattering released at the epoch of recombination. The CMB is isotropic and its average temperature has been measured to high precision and is about 2.72K[8]. Further observations of the CMB and analysis of the temperature maps reveals an anisotropy on the order of $\frac{1}{1000}$ of the average temperature. The inflationary cosmological model suggests that the universe underwent a period of rapid expansion known as inflation. Rapid expansion of space-time is predicted to have sourced gravitational waves which would have imprinted themselves on the polarization of the CMB. Quantum fluctuations are theorized to have sourced scalar density fluctuations which are responsible for the structure we see in the universe and is a contributor to the CMB anistropy. The next sections introduce necessary polarization formalism. Then I briefly go over sources of polarization in the CMB, the polarized foregrounds, and the power spectrum of the CMB.

2.3 Polarization Vector Basis

A discussion of the polarization of the CMB and Galactic foregrounds calls for the introduction of formalism. A common convention used to describe the polarization state of radiation in radio astronomy and the one we will adopt in this paper is the Stokes parameters. The interesting B and E mode field decomposition of the polarization field arises from the differentials of the Stokes Q and U. The Stokes formalism lays the mathematical frame work we will use to work with polarization data.

2.3.1 The Stokes Parameters: T, Q, and U

The Stokes parameters; T, Q, and U are often used to describe the polarization field over the sky. They are defined in terms of linear combinations of electric field polarization basis where the choice of linear or circular basis is arbitrary. Figure 2.1 depicts the IAU convention used to describe the polarization field from Earth's frame of reference. We adopt the IAU convention for the purpose of our simulations.

2.3.2 The E and B Polarization Field Decomposition

The primordial signals are better described by the E and B mode signals imprinted on the relic CMB radiation. The B and E fields are related to the Stokes parameters through their differential. The E and B fields are analogous to the Helmholtz E and B fields decomposition in electrodynamics with an important distinction. The polarization field is a spin-2 vector field meaning a vector rotated by 180° is identical to the un-rotated vector. There is an analogous theorem for spin-2 vector fields which uniquely describes the field as combination of parity even "divergence" like field, the E-mode, and a parity odd "curl" like field, the B-mode. Figure 2.2 depicts and example decomposition of a field into the E and B mode.

2.4 Sources of CMB Polarization

The CMB polarization encodes information about the primordial universe. I will briefly summarize the two main polarization mechanisms of the the CMB and a possible leakage source between observed E and B modes.

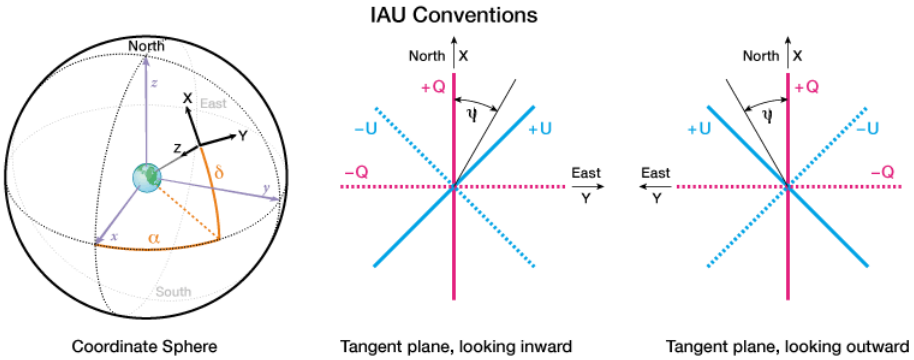

Figure 2.1: Left: a diagram of the coordinate sphere. In the middle of the sphere is the earth. The grey coordinate system is rigidly attached to the earth with z pointing in the North pole direction, x pointing towards the Vernal Equinox, and y is pointing in the direction which completes a right handed coordinate system. The coordinate system in black corresponds to the polarization coordinate system used by an observer looking at the sky from earth. Middle: we see a tangent plane view of the polarization axis for as seen by an observer looking inward i.e. from the sky n earth. Right: we see the tangent plane of the polarization frame as seen by an observer looking outwards. The solid and dotted pink lines correspond to positive and negative Q. At 45° counter clock wise in blue are the positive and negative Stokes U. The angle ψ is a measure of angular distance from a fixed point (this is the angle we use to describe the roll angle of the telescope). The x axis of the polarization basis is pointing up/ North and the y axis points left/ East.

2.4.1 Gravitational Waves

Gravitational waves induce a metric perturbation in the field. These tensor metric perturbations imprint themselves in the polarization state of the travelling CMB photons. Only the presence of gravitational wave can source the "curl" pattern in the CMB polarization field.

2.4.2 Scattering

Quantum fluctuations prior to inflation seeded density perturbations in the scalar field. The quadruple pattern of over and under densities induces a linear polarization due to the Thompson scattering of photons coming from

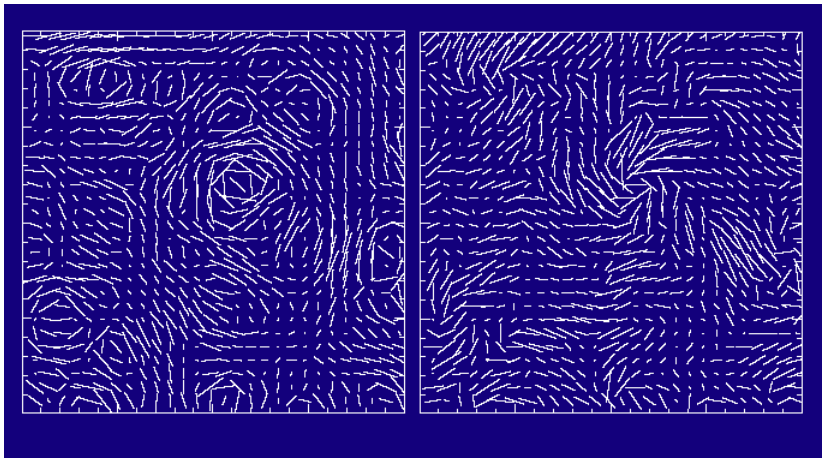

Figure 2.2: On the left is the E field of the input polarization field. Note that prominent large scale structure formed by the filaments is predominantly circular. A symmetric reflection of such structure will result in the same image. This is the parity even behaviour characteristic of the E field. On the right is the B field component of the polarization field. The large scale structure of the filaments does not exhibit the same symmetry. If we reflect the B mode pattern we will see a mirror image. This is the parity odd behaviour of the B field. [Dr. Wayne Hu]

under and over dense areas. These produce a characteristic "divergence" like E mode patterns in the incoming CMB radiation as the electrons can be thought of as "sources" and "sinks" analogous to electric fields of point charges in electrostatics. Figure 2.2 shows a cartoon of the scattering mechanism in the context of quadropole anisotropy.

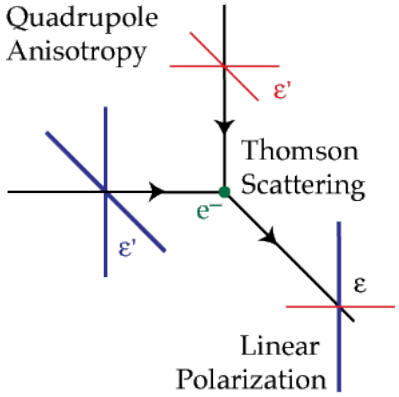

Figure 2.3: A photon incoming from the top(red) has a higher energy and scatters off the electron via Thompson scattering. The scattered photon then travels in the direction out of the page with polarization that is transverse to its initial propogation direction. The cooler (blue) photon scatters off the electron and travels out of the page also polarized in the direction transvers to its initial propagation direction. The superposition of the scattered photons has is net linearly polarized as a result of the peculiar scattering pattern produced by the quadropole anisotropy. [Credit: Dr. Wayne Hu]

2.4.3 Gravitational Lensing

Gravitational lensing a result of the interaction of light with a strong gravitational field. Massive objects such as galaxy clusters can potentially bend the path of photons travelling to us from a source behind the cluster. Thereby acting as a lens that projects the light and remaps the polarization field out the output of the lens. A mixing of Stokes parameters occurs due to the remapping of polarization field which mixes the E and B decomposition of polarization. Gravitiatonal lensing sources additional B mode in the CMB field on smaller angular scales.

2.5 Polarized Galactic Emission

2.5.1 Syncrotron Radiation

Synchrotron radiation is a well known contributor polarized Galactic emission[12]. The physical process that produces Synchrotron radiation requires two components: strong magnetic fields, and relativistic charged particles. A relativistic charged particle will accelerate in the presence of a magnetic field. The accelerating particle will radiate linearly polarized photons. Synchrotron radiation follows a non-thermal power law and its spectral index has been analyzed and characterized. The average spectral index of Synchrotron radiation is approximately $\beta = -3.1$[12].

2.5.2 Thermal Dust

Diffuse emission from dust grains in the interstellar medium is a large contributor to polarized emission in the 20–200 GHz window where CMB is measured [1]. The polarized emission of dust grains depends on their intrinsic shape[14]. Silicates and graphite are strong candidates for the composition of Galactic dust. Figure 2.3 compares the combined polarization amplitude of Thermal Dust and Synchrotron to the expected CMB polarization amplitude in the GHz regime.

2.5.3 Anomalous Emission (Spinning Dust)

Anomalous emission is a postulated mechanism where charged dust grains spin and emit radiation. The evidence for this emission mechanism came from the excess brightness observed that cannot be unaccounted for solely by Hα correlated free-free emission[11]. The anomalous emission is expected to drop off at lower frequency however its spectral and spatial distribution is not well known. Anomalous emission may or may not be polarized and a better understanding of its behaviour requires measurements at more frequencies.

2.6 The CMB Power Spectrum

The spherical harmonic decomposition of the CMB polarization and temperature fields relate observed brightness to spatial distribution. The CMB B mode sourced by gravitational waves is expected to produce large angular scale patterns and drop off at lower angular scales. Gravitational lensing leaks E mode power to observed B mode power at smaller angular scales, corresponding to sources like galaxy clusters. Power spectrum analysis is

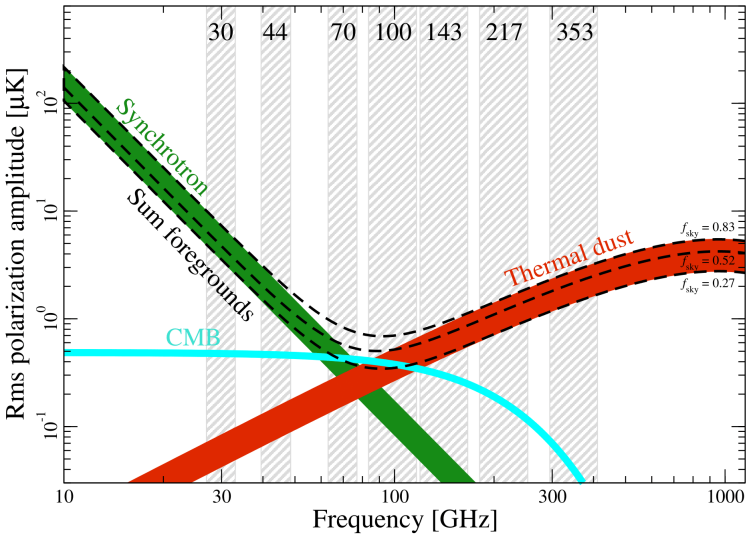

Figure 2.4: A plot of rms amplitude of polarized foreground components in the 10-1000GHz range. The green line corresponds to the Synchrotron polarization amplitude and appears to drop off as frequency increases from 10 to 100GHz. This is in agreement with our power law estimate with average spectra index $\beta = -3.1$. The red line corresponds to the thermal dust amplitude and its overall shape is concave down. The thermal dust emission appears to dominate the polarized foreground after 100GHz. The dashed traces correspond to the sum of polarized foregrounds. It is important to notice that the CMB polarized emission (mint) never outshines the sum of foregrounds even at its minimum around 100GHz capturing the importance of accurate foreground separation. Anomalous may be a contributor to polarized emission in this frequency window however the degree of its polarization is not well understood. [arXiv:1807.06208]

further covered in section 3.3. Figure 2.5 depicts BB auto correlation power spectrum of the CMB given r = 0.1.

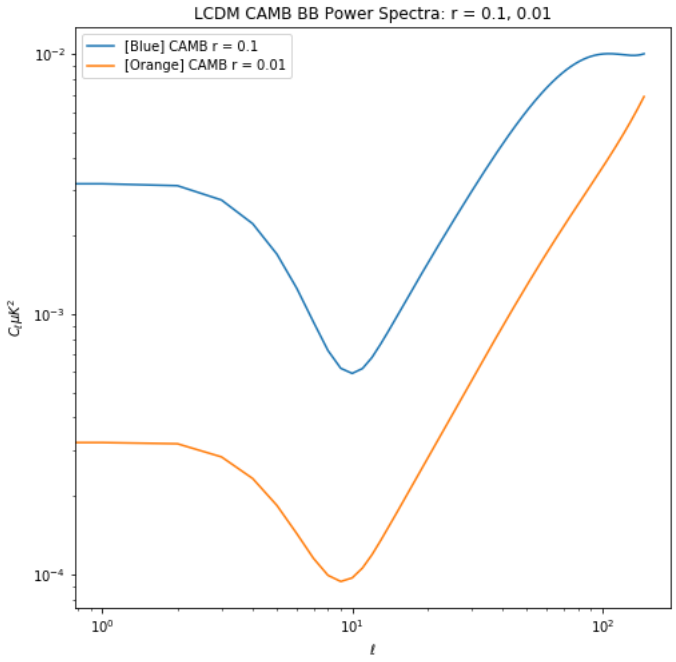

Figure 2.5: Two realization of the CMB BB power spectrum computed using the Code for Anisopropies in the CMB (CAMB). CAMB produces power spectra with ΛCDM as the underlying cosmological model. The blue curve corresponds to realization of the universe with tensor level that is 10 times larger then the one of the orange curve. The higher tensor level in the r = 0.1 realization of the sky increases the BB power of the CMB as compared to the orange curve (r = 0.01). The relation between angular extent and multipole ℓ is approximately: $\frac{\ell}{180^\circ}$. The BB power for both curves drops off between multipoles $2 \leq \ell \leq 10$. This tail corresponds to the BB power contribution of primordial B mode on big angular scales. The BB power then begins increasing for $\ell > 10$ which corresponds to the power contribution of gravitational lensing on small angular scales.

2.6.1 The Tensor to Scalar Ratio r

The tensor to scalar ratio r parameterizes the amplitude of the initial tensor wave and is defined to be the ratio between the initial tensor wave amplitude to scalar field fluctuations amplitude. The current upper limit from the joint analysis of Planck and BICEP2 data is r = 0.044 [16]. It is possible that r = 0 which would corresponds to there being no gravitational waves due to inflation and a zero inflationary B mode contribution to the power spectrum. Although this possibility exists the search for the B mode continues as we learn from previous experiments and instrumentation improves.

2.6.2 BB Power Spectrum Contaminants VS CMB B Mode

Accurate CMB B mode measurements are challenged by the complexity of the foregrounds and the relative brightness of CMB to the foregrounds. The CMB polarized rms temperature is expected to be lower than the combined foreground polarized rms temperature even at the foreground minimum at around ($\nu_{min} = 100GHz$). The task is further complicated by the gravitational lensing mechanisms that can leak E mode power to the measure B mode power. The BICEP collaboration reported a possible detection of the primordial B mode signal [3], but subsequent joint analysis of the BICEP and Planck collaborations found "strong evidence of dust and no statistically significant evidence for tensor modes" [2]. High polarization fidelity maps across a wide frequency range are essential for a reliable foreground decomposition. As future experiments continue to cover a wider range of frequency with high signal purity our B mode detection capability is enhanced.

Chapter 3

Experimental Methods

3.1 The Canadian Galactic Emission Mapper (CGEM) Telescope

The Canadian Galactic Emission Mapper (CGEM hereafter) is a planned radio telescope that will map the polarized 10GHz Northen sky. The telescope will be built at the Dominion Radio Astrophysical Observatory (DRAO) near Penticton, BC. The main science goal of CGEM is to improve Galactic foreground emission modelling in support of the search for the CMB B mode. CGEM will fill the gap in the low radio frequency regime and will compliment other surveys done in the 2.3GHz-23Ghz range: the S-PASS 2.3GHz survey, C-BASS 5.0GHz survey (no data release to date), and WMAP K band 23GHz survey. Polarized Synchrotron emission is well known to dominate the low radio frequency range. The poorly understood anomalous emission may be a contributor to polarized emission in CGEM's target frequency window. The relative dominance of Synchrotron in the 10GHz range allows for a high signal-to-noise measurement of the signal. CGEM will also help characterize the anomalous emission in brightness and polarization if present. The high signal-to-noise measurement will allow us to better model the behaviour of different Galactic emission components and disentangle them in frequency space.

3.1.1 Instrument Characteristics

The CGEM telescope will be built at the DRAO ($\ell \approx 49^{\circ}N$) which physically limits its field of view to the northern sky. The CGEM group is currently exploring a hat feed antenna with a 4 meter dish as a potential design. This design allows for excellent polarization purity as we can potentially avoid struts and feed legs that obscure the aperture. The telescope will observe the sky at 10GHz with a bandwidth of 20%. The DRAO is a radio quiet valley so radio frequency interference is expected to be minimal compared to other geo-locations. However the rise of communication satellite "super" constellations like SpaceX's Starlink which operates in the

10.7-12.7GHz, overlapping with our observation band, [7] raises concern of contamination of ground based observations [9]. The constellations currently deployed may directly affect our experiment. The radio frequency interference in our observation band (10Ghz±20%) at the planned construction site is yet to be characterized and this measurement is planned for the future. Additionally, CGEM is planned to be shielded from ground pick up with an surrounding ground shield that will also help reduce radio interference. An artist's impression of the the instrument is depicted in figure 3.1. CGEM's target angular resolution is 0.5° degrees with a target sensitivity at 10GHz of $\sigma_{CGEM} = 25 - 100\mu K$ in 1 deg^2. This target sensitivity scales to rms temperature fluctuations on the order of nK when extrapolated to the CMB observation window. The corresponding system temperature is $T_{sys} = 44 - 175K$. CGEM will be equipped with low noise cryogenic circularly polarized receivers. A benefit of such system is the lowering of system temperature which improves sensitivity. Finally, the instrument will be attached to an altazimuth mount. The two degrees of freedom are important for a successful scan strategy which will be further explored in section 3.2.2.

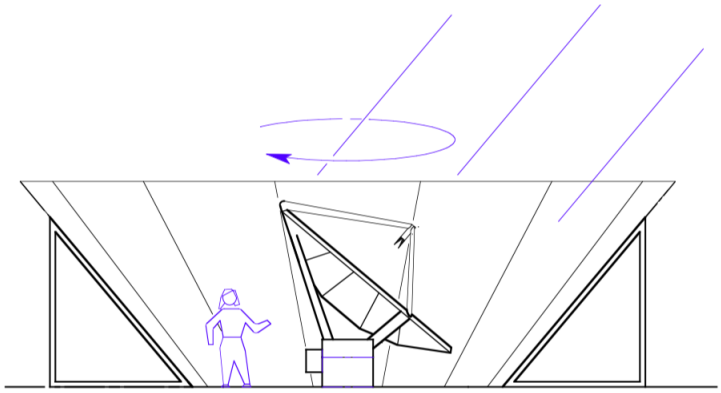

Figure 3.1: A cartoon of a 4-meter dish coupled with a strut supported antenna on an altazimuth mount scanning the sky in azimuth at 4RPM with a fixed zenith angle ($\approx 40°$). [Credit: Dr. Mark Halpern]

3.1.2 Linear VS Circular Antenna Polarization Basis

The choice of the telescope's frame polarization basis is naturally arbitrary. However, we found that the choice of circularly polarized receivers is ad-

vantageous over the linearly polarized receivers. The choice of circularly polarization basis was informed by the lack of noise bias in the correlation product channels involving Stokes Q and U (which contain the interesting polarization for our power spectrum analysis). The signal CGEM will measure is the incoming electric field density weighted with the beam response

$$W_r = \frac{1}{\sqrt{\Omega_r}} \int d^2\hat{n} A_r(\hat{n}, \nu, t)\epsilon(\hat{n}, \nu)$$

$$W_l = \frac{1}{\sqrt{\Omega_l}} \int d^2\hat{n} A_l(\hat{n}, \nu, t)\epsilon(\hat{n}, \nu)$$

Where ϵ is incoming electric field and A_r is the antenna response to radiation polarized in either the LHC(l) or RHC(r) directions (the beam pattern).

3.1.3 Systematic Errors and Stokes Q and U

My project will concentrate on the effect of the beam pattern on polarization observations. The beam pattern and its potential impact on the Stokes parameters is discussed in 3.2.3. A complex system like CGEM has many possible sources of systematic error. The voltages induced at the receiver are amplified which can introduce gain errors in each channel. The electronics can also introduce a phase delay in the either channel. We record voltage correlation products that we then use to recover the observable Stokes parameters. Errors due to electronic effects can directly impact the recovered Stokes T, Q and U. Mechanical errors like motor drift are also possible. In the case that recorded observation direction substantially deviates from the true line of sight the recovered observable correspond to the incorrect sky pixel mixing up the polarization. Electronic effect such as gain and phase errors can be easily added programatically in the current pipe line by operating on the time ordered data.

3.2 Simulator Pipeline

Simulation is a cost effective tool to test the design of complex systems. We programmed a simulator to characterize the performance of realistic mount and hat feed design realizations in Python. This software lays the foundations to the data processing pipeline of the CGEM telescope. The pipeline consists of two main components; the observations simulator, and the map maker. The observations simulator produces realistic time ordered

data for a telescope with an arbitrary: scan strategy, beam co-pol and cross-pol patterns, and other systematic effects such as gain and phase errors. We made extensive use of the Healpy library to implement the observations simulator. The map maker attempts to recover the Stokes T, Q, and U maps from the time ordered data. We aim at constraining systematic effects by comparing their BB power contribution to different levels of expected B mode signal given different r parameters. I will discuss the power spectrum analysis procedure in section 3.4. What follows is an overview of the input data, models, scan strategy, beam pattern, and the output time stream data. Finally, I will discuss the map maker and present simulated CGEM maps with hat feed beam effects.

3.2.1 Input Data and Synchrotron Models

We constructed a simulated sky at 10GHz by scaling the WMAP K band (23GHz) Stokes Q and U maps, and the COMMANDER 408MHz Synchrotron template to $\nu_{CGEM} = 10GHz$ using a uniform spectral index at every pixel. A more sophisticated scaling can be implemented later informed by our own data and other experiments. The COMMANDER map was degraded to NSIDE = 256 to match the resolution of the WMAP K band maps. The brightness of Synchrotron emission is modelled with a power law. The spectral index generally depends on the pointing direction on the sky and frequency. We approximate the Synchrotron power law by assuming no dependence in pointing direction and a uniform spectral index $\beta_s = -3.1$ informed by the average Synchrotron spectral index calculated by the WMAP collaboration[12]. The antenna brightness temperature in every pixel is (where Y denotes the in Stokes map being scaled T, Q, or U):

$$Y_{CGEM} = Y_{in}(\frac{\nu}{\nu_{in}})^{\beta_{CGEM}}$$

All pixels are scaled with the same factor regardless of the true complexity of emission components at a given pixel. This basic model relies on the large relative contribution of Synchrotron to polarized emission in the low frequency range. Thermal dust brightness drops off rapidly in the 10GHz range[4]. An important blind spot of this extrapolation is the unknown frequency response of the anomalous emission component and its overall contribution to the observed polarized emission. We proceed with these assumptions and limitations in mind and feed the scaled input maps to the pipeline.

3.2.2 Scan Strategy

The CGEM telescope is being designed to map the sky with high spatial resolution and high signal-to-noise ratio. A successful scan strategy needs to maximize the the coverage of each sky pixel. Time separated observations of the same pixel under different telescope roll angles are imperative for the map making procedure and reduction of error in the measurement. The CGEM telescope will be be equipped with an altazimuth mount. The suggested scan strategy is a constant speed azimuth scan ($\omega_{azimuth} = 4RPM$) with a constant boresight zenith angle $\phi_{bore} = 40^\circ$. A plot of the bore sight trace given a constant zenith angle and constant azimuth scan is depicted in figure 3.2. To test the performance of the proposed scan strategy we programmed an observations simulator. We used three frames of reference are required to describe the orientation of the telescope relative to the Galactic plane: the CGEM telescope frame, the local DRAO frame, and the Galactic frame. To capture the relative orientation of the three frames we used the Euler angles formalism. The scan strategy was implemented by orienting the telescope bore sight Z_{CGEM} at 40° to the local DRAO zenith, Z_{DRAO}. The constant azimuthal 4RPM rotation was implemented as a successive application a rotation matrix of the CGEM frame with respect to the DRAO frame. The rotation of the earth with respect to the Galactic frame was represented by applying a rotation matrix to the earth frame about its Z_{earth} axis. We produced a hit map assess the performance of the proposed strategy. For a map with resolution NSIDE = 256 and a scan duration of 24 hours all pixels are observed at least once. The map making procedure is discussed in section 2.3.5 where we also present plots of recovered T, Q and U maps. It is also important to consider the potential coverage overlap between surveys. An alternative scan strategy with $\phi_{bore} \approx 60^\circ$ will completely miss the North pole but will cover the latitude range between $-10 \leq \ell \leq 0$. This coverage will complement current CMB experiments conducted in the Southern hemisphere like The Atacama Cosmology Telescope [6] further broadening the frequency coverage crucial for CMB analysis.

3.2.3 The Beam Pattern

The beam pattern of an antenna-reflector pair is a model of its response to radiation from different directions relative to the bore sight. A complication arises from the non-ideal nature of antenna system; an incoming polarized radiation field (co pol) is confused with the orthogonal polarization state (cross pol) due to the imperfect response of the antenna system.

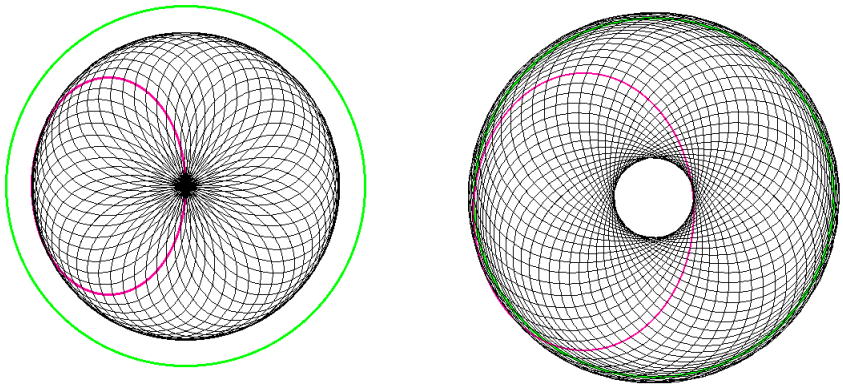

Figure 3.2: Two bore sight pointing traces on the celestial sphere projected onto the plane containing the celestial equator. Left: the green circle denotes equator. The North Celestial Pole comes out of the page through the center of the green circle. In pink is a trace projection of a complete azimuthal scan of CGEM with $\phi_{bore} \approx 40°$. The black circular traces all pass through the North pole and are separated by half an hour. Note the crossing between circles corresponds to the same sky pixel being observed twice under different roll angles. Right: the green circle denotes the equator again. The pink circle corresponds to a projection of a complete azimuthal scan of CGEM. The black circular circles are full azimuthal scan traces separated by half an hour. This is an example of a scan done with zenith angle $\phi_{bore} \approx 60°$. The North pole cap is completely missed in the survey however the scan gains coverage down to latitude ≈ 10. [Credit: Dr. Mark Halpern]

The orthogonal (cross pol) polarization receiver will pick up incoming co pol radiation. The CGEM telescope will be sensitive to Right Hand Circular (RHC) and Left Hand Circular (LHC) polarization as the antenna system cannot be sensitive to only a single mode (RHC/LHC). The current favoured design candidate for CGEM's antenna-reflector pair is a hat feed with a 4m parabolic dish. The main appeal of the hat-feed antenna is the azimuthal symmetry of its beam response. An additional consideration is that an hat feed antenna may be built without aperture obscuring support legs or struts that can cause complex side lobe beam structure [10] which can dramatically impact polarization fidelity. The effect of the co and cross pol response is that an observation of polarization at a given telescope pointing will be a complicated combination of brightness incoming from all directions and

a "bleeding" contribution between the RHC and LHC channels induced by cross-pol pick up. The effect of the beam can be represented as a convolution of the input maps with the beam pattern. The beam response has a direct implication on the observable Stokes T, Q, and U due to mixing of polarization at an observed pixel. GRASP is an antenna reflector design software suite that is capable of modelling antenna systems and their EM response. We obtained a potential hat feet beam pattern from GRASP. A slice of the co and cross pol beam patterns through $\phi = 0$ is depicted in figure 3.3. The co pol response of this antenna system is highly symmetric however the cross pol response's phase is dependent on the telescope's rotation angle. In the case of the co pol response a single convolution is sufficient as the beam pattern is azimuthaly symmetric. The asymmetric cross pol pattern poses a computational challenge as we would have to either: pre-convolve the scaled 10GHz maps with the cross-pol oriented at all rotation angles. Alternatively, we can convolve in real time for a given pointing however the feasibility of this approach is still being assessed. The analysis of the co and cross pol response of the hat-feed antenna design is ongoing. The current version of the pipeline implements the beam convolution under the simplifying assumption that the cross pol is azimuthally symmetric in linear polarization basis. This allows us to proceed with order of magnitude power spectrum analysis as the design progresses.

3.2.4 Mock Time Ordered Data

The data output of the observations simulator is a time stamped array of observation vectors(UNIX time). Each observation vector stores the pointing direction at the time of observation with respect to the celestial frame. The Stokes T, Q and U (μK) observed for the pointing direction. The rotation angle of the telescope (roll angle) with respect to the Galactic frame (degrees). Finally, the observations simulator computes the corresponding voltage correlation product that CGEM would record and stores it in the observation vector. A data flow chart for the observations simulator is presented in figure 3.4. The data structure and pipeline closely simulate the data throughput of CGEM and lay the data processing software foundation. The observations data set is then passed to the map maker to recover the polarization maps as seen by CGEM.

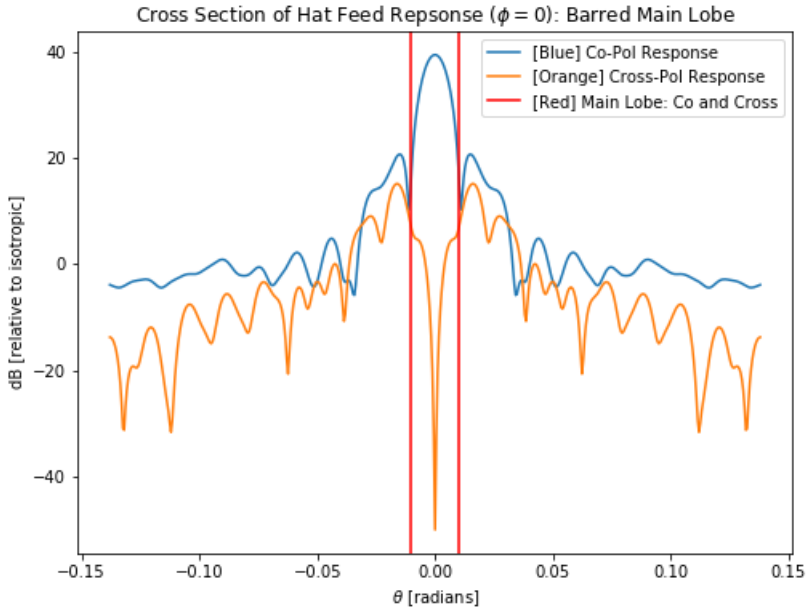

Figure 3.3: Traces of the GRASP hat feed antenna co and cross pol beam patterns scaled to 10GHz in DBi through the $\phi = 0$ plane. In blue is the co pol response of the example hat feed antenna. In orange is the cross-pol response of the antenna. The red vertical lines bar the main co and cross pol lobes which extend between $-0.01 \leq \theta \leq 0.01$. The co and cross pol exhibit similar morphology in the angular range between $-0.05 \leq \theta \leq 0.05$ excluding the main lobes. Note that the cross pol response is not circularly symmetric in either the linear or circular basis: the cross pol response picks up a ϕ dependent phase. The co pol response appears to be circularly symmetric in either basis. We are interested in the effect of the off bore sight $(\theta, \phi = 0)$ response on the polarization maps and particularly the BB/EE power leakage.

3.2.5 Map Making

The map making procedure inverts the voltage correlation products recorded by the instrument to recover the observable Stokes T, Q and U. The map maker combines time separated observations of the same pixels under different rotations angles to recover the Stokes parameters at the pixel. The

recovery of the Stokes T, Q and U from the time stream data can be done using a linear least square method. The map maker was coded by my CGEM collaboration colleague Josh MacEachern. I treat map maker as a black box and feed the time stream data to recover simulated CGEM stokes maps. I present recovered T, Q, and U maps in figure 3.5 that include systematic effect from the full hat feed co and cross pol beam patterns.

3.3 Power Spectrum Analysis

The power spectrum of the E and B polarization field maps relates the signal strength to angular extent across the sky. First, the temperature maps are decomposed into spherical harmonics

$$T(\theta, \phi) = \sum_{\ell, |m| < \ell} a_{\ell m} Y_{\ell m}(\theta, \phi)$$

The C_ℓ's are the expectation of $a_{\ell m}$'s and the $Y_{\ell m}$'s are the spherical harmonics defined in spherical coordinates. The relation between angular extend and the multipole ℓ is approximately $\frac{\ell}{180^\circ}$. Higher ℓ values correspond to smaller angular scales across the sky or finer structure, while smaller multipoles correspond to large scales where $\ell = 0$ corresponds to the average value of the map and ℓ is the dipole moment. The Healpy library provides a robust framework to compute the C_ℓ's of Stokes maps. This decomposition can be applied to the E and B decomposition maps to obtain the auto correlations BB and EE.

3.3.1 Extrapolating Mock 10GHz Observations

We applied a symmetric Galactic cut mask rejecting pixels between $|\ell| < 20^\circ$. The Galactic mask suppresses the bright Galactic plane. Rejected pixels were denoted with 0's in the corresponding index and passed pixels were masked with 1's. As the latitude coverage of CGEM is bound between $9.32^\circ \leq \ell \leq 89.32^\circ$, the pixel coverage is not exhaustive. Pixels that are not observed are masked as NaN and later denoted with 0's in the final masking. The mask can be represented as a window function in map space. Setting pixels to 0 causes a loss of power proportional to f_{sky}, where f_{sky} is the area fraction of sky masked with 1's. We approximated $f_{sky} = \frac{passedpixelscount}{totalpixelscount}$. The calculated power spectra will be scaled by $\frac{1}{(f_{sky})^2}$ to account for the mask. We extrapolate the recovered Stokes T, Q and U maps to $\nu_{target} = 150GHz$ using the same uniform spectral index scaling we applied to the

input maps. The target frequency ν_{target}, corresponds to the frequency window where polarized foreground sum is minimum.

3.3.2 BB Power Auto-Correlations

After masking and extrapolating the mock CGEM maps to the CMB observation frequency window we computed the power spectra of the maps using the Anafast routine from the Healpy library. Anafast is a routine that calculates calculates the TT, EE, BB, TE, EB, TB power spectra of input Stokes T, Q, and U maps where the E and B decomposition happens in the background. We computed the BB auto correlations for the following combinations of hat feed effects: full co and cross pol, and full co pol without cross pol. We also computed the BB power spectra for the input maps convolved with a Gaussian corresponding to the main beam of the hat feed beam pattern. The power spectra are then scaled by $\frac{1}{(f_{sky})^2}$ to account for the masked pixels. We used the Code for Anisotropy in the Microwave Background (CAMB) to compute realizations of the CMB BB power spectrum given two different parameterization of the initial tensor-to-scalar ratio: $r_{1,2} = 0.1, 0.01$.

3.3.3 Δ BB Power Contribution of Systematic Errors

We analyze the difference between BB auto correlation calculated for the recovered CGEM maps with beam effects ($C_{be}(\ell)$) and the error-free input maps smoothed to the CGEM resolution BB power spectra ($C_{sf}(\ell)$). I denote the difference of the power spectra with:

$$\Delta C(\ell) = C_{be}(\ell) - C_{sf}(\ell)$$

We then compared the effective BB power spectrum contribution of the beam effect to the expected CMB BB power spectrum for different r levels. For the CGEM polarization survey to be useful to the CMB B mode search, the effective r level of the systemic's contribution to the BB power spectrum must be lower than the current upper bound of r = 0.44[16].

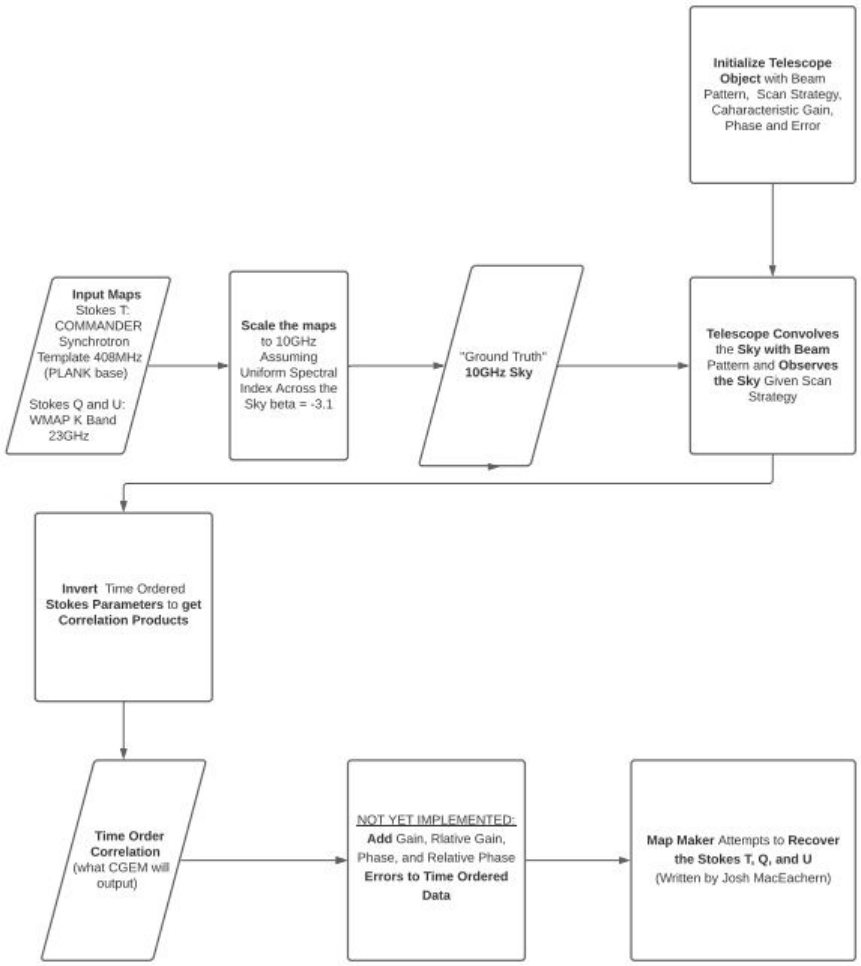

Figure 3.4: A data flow chart through the current version of the CGEM pipeline. The input Stokes T COMMANDER Synchrotron map and the WMAP K band stokes Q and U maps are scaled to 10GHz using a uniform spectral index $\beta = -3.1$. The maps are passed to a telescope objects that knows about its scan strategy and instrumental errors. The telescope convolves the maps with its beam pattern and observes the sky given the scan strategy. The simulator then inverts the observed Stokes T, Q, and U to get voltage correlation products. The data for each observation are stored with the corresponding time stamp, pointing vector, and roll angle of the telescope. Voltage and phase errors can be introduced into the correlation products however this is not yet implemented. The time stream data is then fed to the map maker that attempts to recover the Stokes T, Q and U maps.

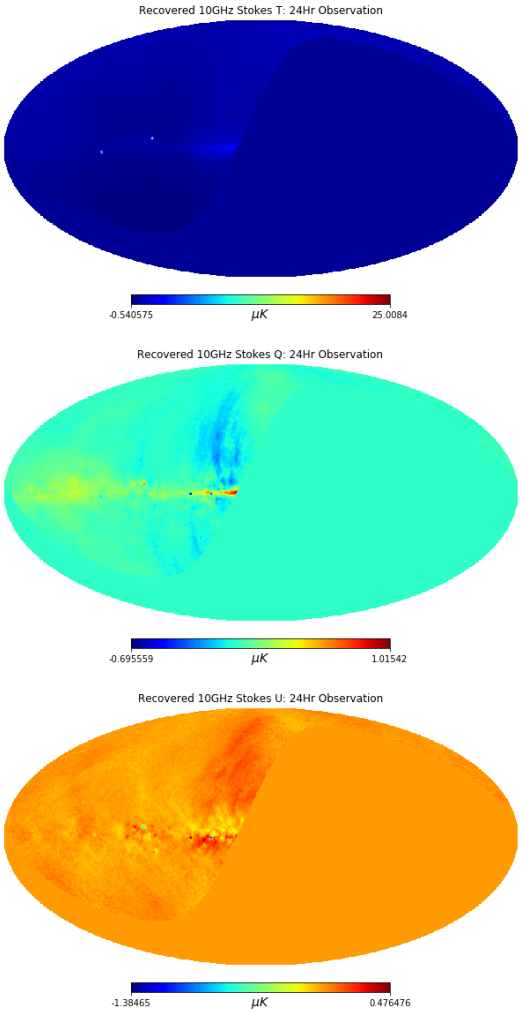

Figure 3.5: I present a set of simulated CGEM T, Q and U maps with the hat feed co and cross pol beam effect incorporated into the simulator. The maps are mollweide projections of the observed thermodynamic temperatures (μK) in Galactic coordinates. The maps were recovered from time ordered data of a 24 hour long scan. The scan strategy used for these simulated observations is a constant azimuth velocity scan (4RPM) with constant zenith angle (= 40°). On top: Stokes T map, middle: Stokes Q map, and bottom: Stokes U map.

Chapter 4

Results

We present plots of the full set of BB power spectra in figure 4.1. The power spectra computed for the main lobe effect, the full co and cross pol beam pattern, and only the full co pol pattern effects, all lie between the CAMB CMB B mode spectra for $0.1 \leq r \leq 0.01$ and $\ell \leq 10$. The BB power contribution of the hat feed full co and cross pol response is on the order of less than $10^{-3}\mu K$ for $\ell \leq 10$ when compared to the isolated main lobe effect. For $\ell > 10$ the CGEM power spectra fall below the CMB B mode C_ℓ's reaching a difference of approximately $10^{-5}\mu K$ at $\ell \approx 100$. The power spectra corresponding to the full co and cross pol and full co pol deviate from the power spectra of CGEM maps with only the main lobe contribution for $\ell > 60$.

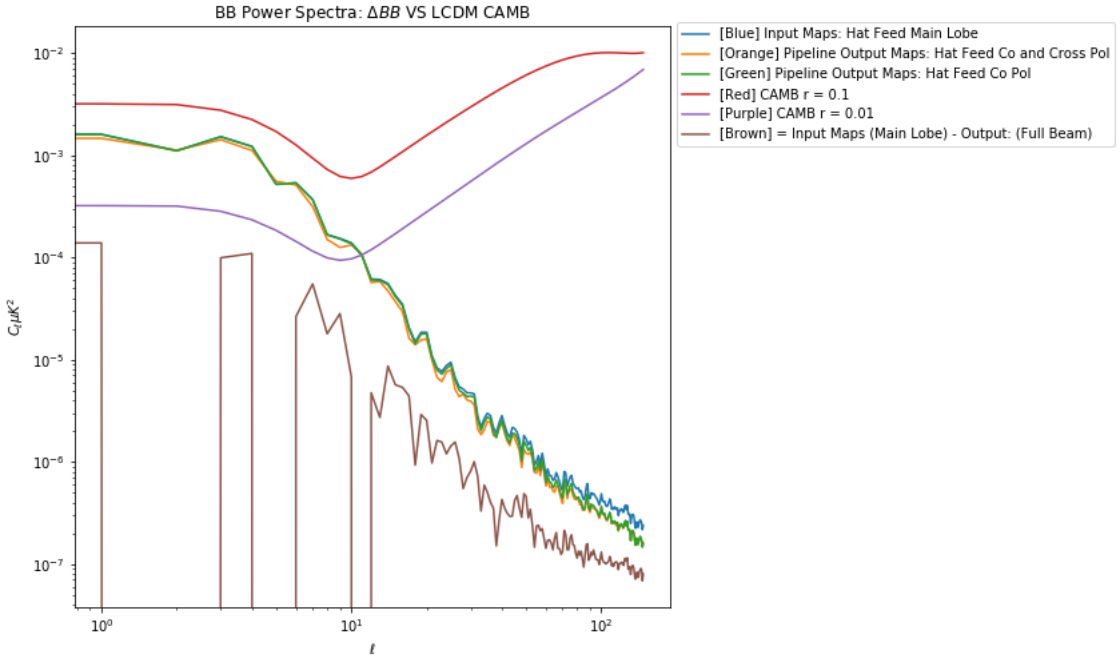

Figure 4.1: Plotted are two sets of CMB power sepctra in log-log space. The red and purple plots are computed using CAMB and they correspond to realization of the CMB BB power spectrum of the Λ CDM model given r = 0.1, 0.01. The blue, orange, and green plots are power spectra of CGEM maps with different simulated beam effects. The brown plot is a the different in power between the input map BB power spectrum and the BB power spectrum of simulated CGEM maps contaminated with the full hat feed co and cross pol effects. The CGEM simulated maps BB power level for $\ell \leq 10$ is bound between the CAMB power spectra for $0.1 \leq r \leq 0.01$. The CGEM power spectra for $\ell > 10$ appear to follow a linear trend. A linear trend in log-log space is indicative of a power law behaviour with respect to ℓ. The decrease in power at $\ell > 10$ can also be accounted for by smoothing of the Q and U maps by the WMAP K band beam. The brown plot is the difference of BB power of the input maps smoothed by the hat feeds main lobe and the output maps of the simulator that are convolved with the full beam pattern. The difference appears to be at most $10^{-4}\mu K^2$ for low ℓ and the difference is 0 for some $\ell < 10$ which is seen in the plot as sharp vertical dips in the brown plot. Further investigation is required to determine whether the beam pattern leaks BB power into EE power making it lower than the input maps for $2 \leq \ell \leq 150$. The possibility of a programmatic error in the pipeline also needs to be eliminated. Overall, the effect of the full beam pattern appears to be extremely moderate for $2 \leq \ell \leq 150$.

Chapter 5

Discussion

The computed BB power spectra for different beam contributions strikingly agree both in shape and behavior over the range of $2 \leq \ell \leq 150$. The presented log-log plot of CGEM power spectra is approximately linear for $\ell > 10$. The CGEM spectra fall within the CMB B mode (r = 0.1, 0.01) for low multipoles $\ell < 10$. The power spectra of the mock CGEM maps starts to drop off rapidly after multipole $\ell = 10$. The rapid drop off in all CGEM power spectra is due to two independent effects. First, the WMAP beam smooths the maps and suppresses power at higher ℓ. Second, galactic emission follows a power law in C_ℓ space with a negative spectral index. The power contribution of the full co and cross pols is on order of $10^{-4}\mu K^2$ for low multipoles $\ell < 10$ and drops off to order of magnitude of 10^{-7} for higher ℓ. The difference of $C\ell$ between the CGEM maps with only the co pol main lobe and the full co and cross pol effects is positive for all ℓ's. The effect of the full hat feed pattern[1] appears to decrease the BB power in simulated observations. Whether this BB power leaks to EE power is unclear and further inquiry is necessary. Further testing of the power spectrum recovery procedure is also needed to eliminate programmatic errors as the source the drop in BB power. We can also feed a map that is purely BB or EE dominated to quantify the systematic effect of the beam and characterize any leakage between caused by the instrument. This analysis is planned for future iterations of the pipeline.

[1]The possible unknown effect of implementing the cross-pol pattern as if it was circularly symmetric lingers and its impact on the power spectra is unknown. The phase if the cross-pol pattern depends on the *phi* plane cross section.

Chapter 6

Conclusion

This project set up the software frame work for simulating realistic polarized sky observation and setting systematic requirements on CGEM. The current version of the simulator pipeline is capable of producing time stream data given a beam pattern and scan strategy. The map making procedure successfully inverts the time stream data and produces Stokes T, Q and U maps of the 10GHz northern sky. The data analysis pipeline successfully masks and computes power spectra of mock CGEM output maps which allows us to assess the level of BB power contamination due to systematic effects. The presented power spectrum analysis suffers from two main caveats: Firstly, the cross pol response of the beam was incorporated as if it was circularly symmetric. We know that the cross pol response is not circularly symmetric in either the circular or linear polarization basis from the analysis of the GRASP hat feed example. Future iterations of the pipeline need to correctly implement the cross pol response whether by pre-computation of or real time computation of convolutions. The approach to this problem is to be determined. Secondly, it is still an open question whether or not such a system is realizable. The analysis in this thesis showed that a telescope scanning the 10GHz sky given CGEM's proposed scan strategy and a realistic hat feed pattern can produce Stokes T, Q, and U maps that are potentially useful for foreground removal. And that the systematic contribution of the full co and cross pol beams to the BB power spectrum is at worst an order of magnitude lower ($10^{-4}\mu K^2$) than the expected B mode level for r = 0.01 ($10^{-3}\mu K^2$) at low multipole $\ell \leq 10$. This preliminary analysis of the performance of the hat feed antenna solidifies it as the leading design choice for CGEM. The current pipeline can be further utilized to assess the impact effects of more systematic driving the CGEM design effort forward.

Bibliography

[1] A. Abergel, P. A. R. Ade, N. Aghanim, M. I. R. Alves, G. Aniano, C. Armitage-Caplan, M. Arnaud, M. Ashdown, F. Atrio-Barandela, and et al. Planck2013 results. xi. all-sky model of thermal dust emission. *Astronomy Astrophysics*, 571:A11, Oct 2014.

[2] P.A.R. Ade, N. Aghanim, Z. Ahmed, R.W. Aikin, K.D. Alexander, M. Arnaud, J. Aumont, C. Baccigalupi, A.J. Banday, D. Barkats, and et al. Joint analysis of bicep2/keck arrayandplanckdata. *Physical Review Letters*, 114(10), Mar 2015.

[3] P.A.R. Ade, R.W. Aikin, D. Barkats, S.J. Benton, C.A. Bischoff, J.J. Bock, J.A. Brevik, I. Buder, E. Bullock, C.D. Dowell, and et al. Detection of b-mode polarization at degree angular scales by bicep2. *Physical Review Letters*, 112(24), Jun 2014.

[4] Y. Akrami, M. Ashdown, J. Aumont, C. Baccigalupi, M. Ballardini, A. J. Banday, R. B. Barreiro, N. Bartolo, S. Basak, and et al. Planck2018 results. *Astronomy Astrophysics*, 641:A4, Sep 2020.

[5] Daniel Baumann. Tasi lectures on inflation, 2012.

[6] Steve K. Choi, Matthew Hasselfield, Shuay-Pwu Patty Ho, Brian Koopman, Marius Lungu, Maximilian H. Abitbol, Graeme E. Addison, Peter A. R. Ade, Simone Aiola, David Alonso, and et al. The atacama cosmology telescope: a measurement of the cosmic microwave background power spectra at 98 and 150 ghz. *Journal of Cosmology and Astroparticle Physics*, 2020(12):045–045, Dec 2020.

[7] Federal Communications Commission. Application For Approval for Orbital Deployment and Operating Authority for the SpaceX NGSO Satellite System. March 2018.

[8] D. J. Fixsen. The temperature of the cosmic microwave background. *The Astrophysical Journal*, 707(2):916–920, Nov 2009.

[9] Stefano Gallozzi, Marco Scardia, and Michele Maris. Concerns about ground based astronomical observations: a step to safeguard the astronomical sky, 2020.

[10] Andrew Hunt and Alan Wright. Complex, off-axis sidelobes of a radio telescope caused by feed-support legs. , 258(1):217–224, September 1992.

[11] A. Kogut. Anomalous microwave emission, Feb 1999.

[12] A. Kogut, J. Dunkley, C. L. Bennett, O. Dore, B. Gold, M. Halpern, G. Hinshaw, N. Jarosik, E. Komatsu, M. R. Nolta, and et al. Three-year wilkinson microwave anisotropy probe(wmap) observations: Foreground polarization. *The Astrophysical Journal*, 665(1):355–362, Aug 2007.

[13] A. A. Penzias and R. W. Wilson. A Measurement of Excess Antenna Temperature at 4080 Mc/s. , 142:419–421, July 1965.

[14] A. Prunet, S. Lazarian. Polarized foreground from thermal dust emission, Feb 1999.

[15] G. Rocha, A. J. Banday, R. Belen Barreiro, A. Challinor, K. M. Górski, B. Hensley, T. Jaffe, J. Jewell, B. Keating, A. Kogut, C. Lawrence, G. Panopoulou, B. Partridge, T. Pearson, J. Silk, P. Steinhardt, I. Whehus, J. Bock, B. Crill, J. Delabrouille, O. Doré, R. Fernandez-Cobos, A. Ijjas, R. Keskitalo, A. Kritsuk, A. Mangilli, L. Moncelsi, S. Myers, B. Steinbach, and M. Tristram. Astro2020 apc white paper: The need for better tools to design future cmb experiments, 2019.

[16] M. Tristram, A. J. Banday, K. M. Górski, R. Keskitalo, C. R. Lawrence, K. J. Andersen, R. B. Barreiro, J. Borrill, H. K. Eriksen, R. Fernandez-Cobos, and et al. Planck constraints on the tensor-to-scalar ratio. *Astronomy Astrophysics*, 647:A128, Mar 2021.